Advanced Fiber Materials (2022) 4:908–922
https://doi.org/10.1007/s42765-022-00154-7

RESEARCH ARTICLE

# Photothermal-Triggered Structural Change of Nanofiber Scaffold Integrating with Graded Mineralization to Promote Tendon–Bone Healing

**Chenghao Yu[1,2] · Tianrui Wang[1] · Hongcui Diao[5] · Na Liu[2] · Yi Zhang[1] · Hongyuan Jiang[1] · Peng Zhao[1] · Zhengyi Shan[1] · Zewen Sun[1] · Tong Wu[2,3] · Xiumei Mo[4] · Tengbo Yu[1]**

Received: 22 December 2021 / Accepted: 15 February 2022 / Published online: 22 April 2022


## Abstract

Scaffolds functionalized with graded changes in both fiber alignment and mineral content are more appealing for tendon-bone healing. This study reports the healing of rotator cuff injury using a heterogeneous nanofiber scaffold, which is associated with a structural gradating from aligned to random and an increasing gradient of mineral content in the same orientation. The photothermal-triggered structural change of a nanofiber scaffold followed by graded mineralization is key to constructing such scaffolds. This type of scaffold was found to be biocompatible and provide beneficial contact guidance in the manipulation of tendon-derived stem cell morphologies in vitro. Specifically, tenogenic and osteogenic differentiation of tendon-derived stem cells were simultaneously achieved using the fabricated scaffold. In vivo investigation also showed the improved healing of rabbit rotator cuff injuries based on immunohistochemical analysis and biomechanical investigation that indicates the promising potential of a dual-gradient nanofiber scaffold in clinical tendon-bone healing.

**Keywords** Photothermal welding · Graded mineralization · Nanofiber scaffold · Tendon-derived stem cells · Tendon-to-bone healing

## Introduction

Rotator cuff tears are one of the most common sports injuries, often causing individual symptoms including pain, weakness, stiffness, and a limited range of mobility of the shoulder, which eventually pose significant financial burden on society [1]. Treatment for symptomatic rotator cuff tears is usually based on surgical repair. Although some patients may experience a significant improvement in shoulder function after surgery, the re-tear rate is sometimes high, ranging from 15 to 94% [2, 3]. This is due to lack of regeneration of the complex soft-to-hard structure and low tissue strength resulting from the scar healing at the tendon-bone interface [4, 5]. In this regard, surgical management of rotator cuff tears remains a challenge, and better methods to avoid re-tears must be developed.

Tendon-bone tissue engineering has received increasing attention as a novel treatment strategy. Tissue engineering, which aids in tendon-bone tissue healing, can imitate natural tissues and provides a suitable extracellular matrix environment (ECM), which is essential for tissue repair. The ECM microenvironment of the cellular niche is crucial

✉ Tong Wu
twu@qdu.edu.cn

✉ Tengbo Yu
ytb8912@hotmail.com

1 Department of Sports Medicine, Affiliated Hospital of Qingdao University, Qingdao 266061, Shandong, China

2 Institute of Neuroregeneration and Neurorehabilitation, Qingdao Medical College, Qingdao University, Qingdao 266071, Shandong, China

3 Shandong Key Laboratory of Textile Materials for Healthcare, Collaborative Innovation Center for Eco-Textiles of Shandong Province and the Ministry of Education, 308 Ningxia Road, Qingdao 266071, Shandong, China

4 State Key Lab for Modification of Chemical Fibers and Polymer Materials, College of Chemistry, Chemical Engineering and Biotechnology, Donghua University, Shanghai 201620, China

5 Department of Endocrinology, Jinan Central Hospital Affiliated To Shandong University, No. 105 Jiefang Road, Jinan 250013, Shandong, China

because it can regulate the behavior and fate of stem cells [6]. Decellularized tendon-bone junction tissue has been used for tendon-bone healing to provide an essential ECM microenvironment [7]. Moreover, investigators have endeavored to obtain an optimal strategy to produce biomaterials that mimic the natural tendon-bone tissue structure so as to facilitate tissue regeneration [8]. Scaffolds have been found to promote homologous cell differentiation by mimicking biophysical and biochemical properties present in natural tissues [9]. An ideal tendon-bone tissue repair scaffold is composed of nanofibers arranged uniaxially at one end and randomly at the other end [10, 11]. Furthermore, a hierarchical arrangement of the scaffold with graded changes in porosity and fiber alignment has been introduced to imitate the graded transition in cell morphology at the tendon-bone insertion [12]. Similarly, structures with graduated hardness that simulate changes in mineralization at the tendon-bone interface facilitate osteogenic differentiation of stem cells [13]. Various stem cells have been used in experiments on tendon-bone healing, including bone marrow stem cells (BMSCs) [14], adipose-derived stem cells, and tendon-derived stem cells (TDSCs) [15]. Compared with BMSCs, which have been applied in most of the previous studies, TDSCs have been found to have higher tenogenicity and higher levels of tendon-related factor expression [16].

In our previous study, we reported a method for the photothermal welding of non-woven mats of electrospun nanofibers by introducing a near-infrared (NIR) dye, such as indocyanine green (ICG) [17]. The nanofibers were observed to weld at their cross points or even fuse together under the photothermal effect. The degree of welding can be controlled with adjustment of the power and duration of an NIR laser in different regions, resulting in gradient structural features. Nevertheless, a gradient in hydroxyapatite content exists at the natural tendon-bone interface. Biomineralization has been applied to produce mineral coating on nanofibers to imitate the mineralization gradient [18]. There is a positive correlation between fiber mineralization and the time period for which the fiber is immersed in solution [19]. Thus, the gradient change in the mineralization layer on the scaffold surface can be achieved by controlling immersion time of the scaffold in the solution. This strategy has been successfully applied to generate gradations in mineral content on poly(lactic-*co*-glycolic acid) (PLGA) and polycaprolactone (PCL) nanofibers.

In humans, most rotator cuff tears involve the supraspinatus tendon [20] owing to innate features, for example, the tendon's susceptibility to injury. External factors, such as overuse and repetitive injury also contribute to the high prevalence of supraspinatus injury [21]. External factors are mostly related to the tendons passing through the tunnel formed by the coraco-acromial arch when the humerus is elevated and stimulated. Therefore, an ideal animal model of rotator cuff pathology needs to closely reproduce this external interaction between the tendon and its surrounding skeletal structure. The rabbit subscapularis tendon passes through a similar tunnel, which is considered anatomically, biomechanically, and histologically suitable for studying the pathology and repairing the human rotator cuff [22]. In addition, the rabbit subscapularis footprint was reported to be about one-quarter of the size of the human supraspinatus footprint, allowing researchers to create a rotator cuff tear model [23]. Considering that the nanofiber scaffold is a two-dimensional structure, it may be difficult to repair a full-thickness tear of the rotator cuff. Therefore, we chose a rabbit model of a partial injury of the subscapularis tendon. Some limitations to this model include that the shoulder is a weight-bearing joint for a quadruped animal, unlike in humans, and the model we created is an acute tendon injury, which does not reflect the clinical situation of a chronically torn rotator cuff.

In the current study, we used the photothermal welding technique to generate gradient structures from aligned to random, together with the graded mineralization coating to mimic the natural change in the tendon-bone interface (Scheme 1). This study aimed to investigate the effect of the nanofiber scaffold with dual gradients of fiber alignment and mineral composition on the regulation of TDSCs behaviors in vitro and its healing performance in a rabbit rotator cuff injury model in vivo.

Schematic illustration showing the scaffold modified with dual gradients of both surface structure and mineral content to replicate the native interface between tendon and bone, and its use to facilitate the tendon-bone healing in a rabbit rotator cuff injury model.

## Experimental Section

### Chemicals and Materials

PU was provided by the Biomaterials and Tissue Regeneration Group from Donghua University. ICG was purchased from Tokyo Chemical Industry Co., Ltd (Tokyo, Japan). Hexafluoroisopropanol was acquired from Macklin Biochemical Co., Ltd. (Shanghai, China). The PhalloidiniFluor 488 antibody and rabbit anti-mouse Tenascin C primary antibody were obtained from Abcam (Cambridge, UK). The Cell Counting Kit-8 (CCK-8), rabbit anti-rabbit Collagen I primary antibody, rabbit anti-rabbit Collagen III primary antibody, rabbit anti-rabbit Runt-related transcription factor 2 (Runx2) primary antibody, and goat anti-mouse Alexa Fluor-488 secondary antibody were purchased from Bioss Biotechnology Co., Ltd. (Beijing, China). Dulbecco's modified eagle medium (DMEM), penicillin/streptomycin, collagenase type I, 4',6-diamidino-2-phenylindole (DAPI),

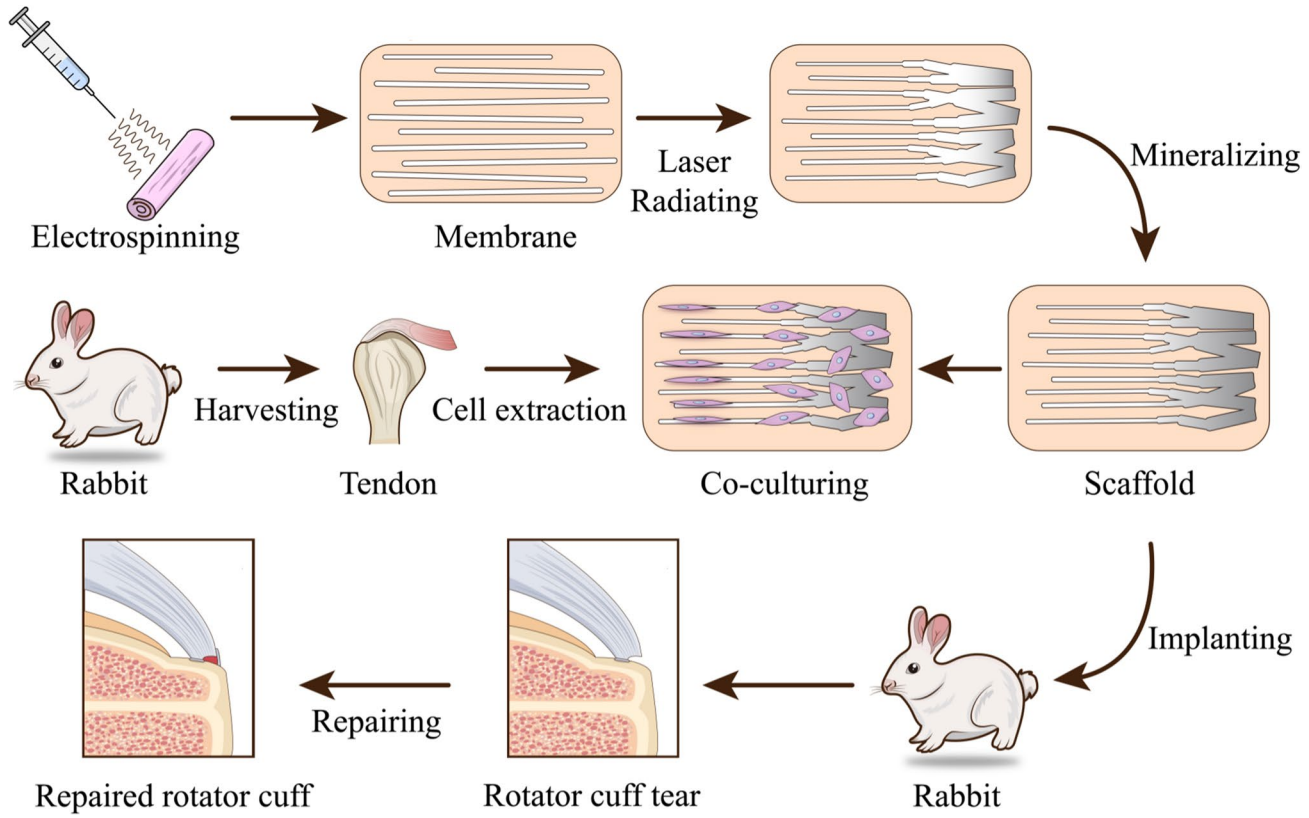


**Scheme 1** Schematic illustration

and goat anti-rabbit Alexa Fluor-594 secondary antibody were bought from Solarbio Science & Technology (Beijing, China). Fetal Bovine Serum (FBS) was purchased from Gibco (California, USA). Dispersase II and trypsin-ethylenediamine tetraacetic acid (EDTA) were acquired from Sigma (Saint Louis, USA). Simulated Body Fluid (SBF) was purchased from Beijing Leagene Biotechnology Co., Ltd. (Beijing, China).

## Fabrication and Characterization of Uniaxially Aligned PU/ICG Nanofibers

The uniaxially aligned nanofibers were fabricated using an electrospinning setup with a high-speed drum. PU was dissolved in hexafluoroisopropanol at a concentration of 8 wt.%, and then ICG was directly mixed into the solution for electrospinning. In the electrospinning process, the solution was aspired into a 5 mL syringe, and subsequently, the syringe was installed onto the electrospinning equipment for spinning. The solution was pumped out at a rate of 0.8 mL/h through a blunt 22-gauge needle. A high voltage (DC) of 18 kV was applied between the needle and a grounded collector separated by 15 cm. A high-speed drum (2500 rpm) was used as the collector to obtain uniaxially aligned nanofibers. The electrospinning process was terminated after 30 min. The sample was coated with Au/Pd using a Hummer 6 sputter (Anatech, CA, USA) and then imaged using a Hitachi 8230 cold field-emission scanning electron microscope (Tokyo, Japan). The average diameter of the nanofibers was measured using ImageJ software from 100 nanofibers in the scanning electron microscopy (SEM) images.

## Photothermal Welding and Mineralization for the Nanofibers

Uniaxially aligned nanofiber scaffolds with ICG content of 0.5% and 1% were prepared. The nanofiber scaffolds were cut into several squares of equal size ($2 \times 2$ cm$^2$ for each sample) and attached to the glass slide with biological glue. They were then irradiated with a laser, which excited the photothermal material (ICG) to produce heat, causing the nanofibers to reach the melting point and be welded. During laser irradiation, the unilluminated areas of the scaffold were covered using a plate with holes, and the temperature of the scaffold surface was observed using a thermal imaging camera. The temperature changes at different light intensities and times were recorded. The nanofiber scaffolds were observed using SEM.

Four structures of the nanofiber scaffolds were selected based on the SEM results, and the selected four structures were mineralized with a coating treatment in the present study. The concentration of the mineralized solution was 10 times that of SBF [18]. The pH of this solution was adjusted between 4.2–4.5 with HCl and NaOH, and then $NaHCO_3$ was added to adjust the pH to 6.5–6.8. The obtained nanofiber scaffolds were placed vertically in a 10 cm diameter dish and slightly fixed. The four structures were immersed in the prepared solution for 0, 0.5, 1, and 2 h separately. After the treatment, the scaffolds were rinsed repeatedly with distilled water and anhydrous ethanol, and the mineralized scaffolds at different times were acquired. SEM was used to analyze the surface morphology of the nanofiber scaffolds.

## TDSC Isolation and Identification

This study was approved by the Institutional Animal Care and Utilization Committee of Qingdao University. The subscapularis tendon of a 4-week-old New Zealand white rabbit was mixed with 1 mL of 0.05% trypsin-(EDTA) to cover and digest the tendon tissue. The complete medium was then used to terminate the trypsin–EDTA reaction. The tendon tissue was cut into small pieces ($1 \times 1 \times 1$ $mm^3$) and digested with a mixture of 3 mL of type I collagenase (3 mg/mL) and 4 mg/mL of Dispersase II. The solution was filtered with a 70 μm cell filter to obtain the remaining cells. These cells were then cultured in T25 culture flasks at 37 °C in the presence of 5% $CO_2$. The culture medium was replaced every 3 days. The cells were passaged after reaching 90% confluence, and the third-generation cells were used in the experiment. The cells were cultured in specific differentiation media to undergo multiple differentiations and identifications of cells. (1) The cells were cultured with adipogenic induction, and maintenance medium for 14 days and oil red staining confirmed the differentiation into adipocytes. (2) The cells were cultured with an osteogenic induction medium for 14 days, and Alizarin Red staining confirmed the differentiation into osteoblasts. (3) The cell pellets were cultured with chondrogenic induction and maintenance medium for 21 days, and Safranine O staining confirmed the differentiation into chondrocytes. The cells were inoculated at the density of 10, 20, 40, and 80 cells/$cm^2$ in a 6 cm-diameter Petri dish for 14–20 days to identify the proliferation and colony formation of the cells. The cells were incubated with the fluorescent primary antibody diluted with phosphate buffered saline (PBS) on ice for 60 min, washed thrice, and then detected using flow cytometry to confirm specific antibodies (SSEA-4 and OCT-4) on the cell surface.

## Cell Viability

The nanofiber scaffolds with different welding extents with or without mineralization were cut to the appropriate size. The scaffolds were adhered to circular glasses with biological glue and then clung to a 24-well plate. The plain glass was used as a control group. After 75% alcohol fumigation for 6 h, the TDSCs were inoculated on the nanofiber scaffolds. The scaffolds were treated with ultraviolet radiation for 0.5 h in the ultra-clean platform. They were washed three times with PBS containing 1% penicillin/streptomycin and separately washed thrice with DMEM. They were then incubated with a 10% complete medium at 37 °C for 1 h. Subsequently, the TDSCs were inoculated into the 24-well plate at $1 \times 10^4$/well for 3 days. The cells were washed with PBS, and the fresh complete culture medium with a 10% CCK-8 reagent was added to each well. After incubation for 3 h, the plate was shaken for 15 min, and the absorbance of the supernatant at 450 nm was measured using a microplate reader.

## Generation of the Nanofiber Mat With Gradations in Both Fiber Alignment and Mineral Content

The four regions in the nanofiber scaffold were arranged in the radial direction. After fabrication, SEM was used to observe changes in the nanofiber structure, which was specified as regions I, II, III, and IV. Region I represented uniaxially aligned nanofibers, regions II and III constituted transition regions, and region IV designated random fibers. The nanofiber scaffold was put in a 10 cm-diameter Petri dish and gently fixed. Region IV of the scaffold was at the bottom, region I was in the upper area, and regions II and III were in the middle. A propulsion pump was used to add mineralization solution into the dish at a rate of 0.5 mL/min for 2–2.5 h. After repeated washing with distilled water and anhydrous ethanol, a bidirectional gradient nanofiber scaffold was obtained. The scaffold with the gradient of fiber alignment caused by photothermal welding was named PW. The scaffold with dual gradients of fiber alignment and mineral composition was named PW + GM. SEM and energy-dispersive X-ray spectroscopy (EDX) were used to observe changes in the nanofiber structure and mineralization content. The scaffolds were also detected by a Bruker atomic force microscope (AFM, Dimension Icon, America).

## Cell Morphology and Differentiation

The nanofiber scaffolds with structural gradient changes before and after mineralization were placed in a 24-well plate and inoculated with TDSCs after sterilization. The CCK-8 test was performed separately after culturing the cells for 1 day, 3 days, and 7 days. After culturing for

3 days, immunofluorescence F-actin/DAPI staining was performed, and changes in cell morphology were observed under a microscope. After culturing the TDSCs for 3 days, the culture medium was removed, and 3% glutaraldehyde was used to fix samples for 30 min at room temperature. After that, 0.1% Triton X-100 was applied to permeate for 5 min, and the samples were washed with PBS thrice. Each sample was mixed with 200 μL of bovine serum albumin (BSA) solution containing 0.1% F-actin and incubated at room temperature for 30 min in the dark. After washing the sample three times with PBS, mounting tablets containing DAPI were added, and the sample was observed under an Olympus IX73 inverted microscope. In the negative control staining, the F-actin staining agent was not added, and the other steps were the same as noted above. ImageJ software was used to measure the length and breadth of the cells at the four regions of the scaffolds.

TDSCs were cultured on the fibrous scaffold with mineralization for 14 days and stained with immunofluorescence Runx2/Tenascin C/DAPI to observe the corresponding protein expression. After 14 days of culturing, the medium was removed. The samples were fixed with 3% glutaraldehyde for 5 min at room temperature and washed three times with PBS. Following that, 0.1% Triton X-100 was used to permeate the cell membrane for 5 min. After washing the samples three times with PBS, the samples were blocked with 1% BSA for 2 h and then again washed with PBS three times. Each sample was mixed with 200 μL of 1% BSA solution containing a 0.1% Runx2 rabbit anti-rabbit primary antibody and 0.5% Tenascin C mouse anti-rabbit primary antibody, and then incubated at room temperature for 2 h. The samples were washed once with 0.1% Tween 20 and twice with PBS. Each sample was mixed with 200 μL of 1% BSA solution containing a 0.5% goat anti-rabbit 594 secondary antibody and 0.5% goat anti-mouse 488 secondary antibody. The samples were incubated at room temperature for 30 min in the dark and then washed once with 0.1% Tween 20 and twice with PBS. Next, mounting tablets containing DAPI were added to each sample, and the samples were observed under the fluorescence microscope. The average fluorescence intensity at each position was calculated from four samples using ImageJ software and then plotted. In the negative control staining, the primary antibody was not added, and the other steps were the same as noted above.

## In Vivo Investigation

All of the in vivo experimental procedures conformed to the institutional guidelines for animal care and were approved by the Animal Ethics Committee of the Affiliated Hospital and Qingdao University. Adult New Zealand white rabbits weighing 3.5–4 kg were used as the experimental animals, and the injuries of subscapularis tendons were applied to the model. First, 24 rabbits were randomly divided into four groups: the photothermal welding plus graded mineralization (PW + GM) group, photothermal welding (PW) group, control group, and normal group. For animal experiments, 75% alcohol was used to fumigate the nanofiber scaffolds of structural gradient changes with and without mineralization overnight. The rabbits were anesthetized by injection of sodium pentobarbital (30 mg/kg). After the left and right shoulders were shaved, Lidocaine Hydrochloride Injection (0.25%) was sterilized into the shoulder for local anesthesia. To establish the bilateral partly rotator cuff tear models, a percutaneous surgical incision of about 3 cm was made on the anterolateral aspect of both shoulders. The subscapularis tendon was found after blunt dissection of the deltoid and supraspinatus muscle. Then, 50% of the thickness of the subscapularis tendon was cut sharply at the location where the tendon was linked to the bone, and the surface stump of the humeral head was cleaned. The nanofiber scaffold with or without mineralization was cut into $1.5 \times 0.6\ cm^2$ in size. Then, the injured tendons were separately covered with the different scaffolds (PW + GM and PW) and fixed at the four corners with sutures. The injured subscapularis tendons served as the control group and the uninjured tendons served as the normal group. The muscles and the skin incisions were closed in layers. The shoulders were bandaged with gauze. After the surgery, penicillin was injected intramuscularly for 3 days. Then, the rabbits were put in cages without restricting their activities.

After 3 and 6 weeks, the shoulder specimens were explanted. The healing status was observed by hematoxylin and eosin (H&E), Masson, Sirius red staining and immunohistochemically staining for collagen I and collagen III. The tissues for histologic analyses were fixed with 10% neutral buffered formalin for approximately 2 weeks, fully decalcified in 5% nitric acid, and then trimmed and embedded in paraffin. The sections (3 μm in thickness) were cut and stained with H&E and Masson. The tissue sections were separately treated by Sirius red staining and immunohistochemical staining of collagen I and collagen III to observe the expression of collagen in the repaired tissues. The percentage of positive areas in Masson and the immunohistochemical staining micrographs were measured and calculated using ImageJ software. Immunofluorescence staining was performed as described earlier to analyze the expression levels of tendon-related proteins in injured tendons. Briefly, the sections were deparaffined, hydrated, inactivated with endogenous peroxidase, repaired with antigens, blocked with 5% normal goat serum, and then incubated overnight at 4 °C using Tenascin C (mouse anti-rabbit 1:1000) and Runx2 (rabbit anti-rabbit 1:500) monoclonal antibodies. This was followed by incubation with the goat anti-mouse 488-conjugated secondary antibody (1:500) and goat anti-rabbit 594-conjugated secondary antibody (1:500) for 1 h.

The sections were mounted using mounting tablets containing DAPI and examined under a fluorescence microscope. The primary antibody was not added in the negative control staining, and the other steps were the same as noted above.

Four specimens were selected from each of the three groups at 3 and 6 weeks. The subscapularis muscle and the proximal humerus were intercepted on both sides. The tendon side was fixed with sandpaper, and the proximal humerus was fixed with a hemp rope. The tensile test was performed on the Instron-3300 universal material testing machine, and the load rate was 0.4 mm/s. The rupture position, maximum load (N), and load of the subscapularis tendon were recorded in detail.

### Statistical Analysis

One-way analysis of variance (ANOVA) was used for multifactor comparison, followed by Student *t* tests for all of the pairwise comparisons. All of the values were averaged at least in triplicate and expressed as the mean ± standard deviation.

## Results and Discussion

### Photothermal Welding of Electrospun Nanofibers to Change the Fiber Alignment

The average diameter of the nanofibers was 683 ± 215 nm. The temperature changes in the mats with 0.5% and 1% ICG content were separately recorded using an infrared camera after irradiation with an 808-nm laser under different power densities (Figure S1). A positive correlation was found between the surface temperature of the nanofiber scaffold and irradiation time. The temperature was observed to rise more promptly with a higher laser intensity with the same irradiation time. Higher ICG content was associated with less time to reach a certain surface temperature under the same laser intensity. The variation pattern is consistent with our previous findings [17]. As the temperature increased, the scaffolds finally melted and broke. From the infrared images, photographs, and SEM observation in Fig. 1A–C, we determined the ICG content (1%) and laser intensity (2 W/cm$^2$) for optimization of the nanofiber structure. The irradiation times set for gradient changes where the fiber oriented from uniaxially to randomly were 0, 5, 8, and 10 s. The final scaffold surface temperatures were 25, 110, 130, and 145 °C.

### Mineralization of Nanofibers with Different Welding Extent

SEM images of PU fibrous membranes after mineralization for different times are displayed in Fig. 1D. After 0.5 h immersion into 10SBF, there were a few apatites observed on these fibers. After 1 h, some apatite clusters appeared on the fiber surface. More apatite clusters with nano-sheet structure were observed on the fiber surface after extending the mineralization time to 2 h. Further, the mineral deposition on the scaffold surface was observed to increase with the immersion time [24]. The preparation of calcium phosphate coating was convenient and fast, and the coating could be formed by 10SBF quickly on the scaffold surface [19, 25].

### Cell Viability on Welded and Mineralized Nanofibers

The extracted TDSCs exhibited classical stem cell characteristics, including clonogenicity, typical surface antigen expression, and multi-lineage differentiation potential. The cells demonstrated a fibroblast-like cell morphology in vitro (Figure S2A). Crystal violet staining indicated that the colonies were formed after in vitro culture for 16 days (Figure S2B–E). The fluorescence activating cell sorter results showed that more than 85% and 90% of surface-specific markers OCT4 and SSEA4 were positive for TDSCs, respectively (Figure S2F and G). TDSCs could be induced to differentiate into chondrocytes, adipocytes, and osteoblasts in vitro (Figure S3). Thereafter, the extracted TDSCs were planted on the obtained nanofiber scaffold to verify its cytocompatibility. The results indicated that relative viability of the TDSCs at 72 h was close, which means that PU fiber membrane and calcium phosphate coating did not show obvious cytotoxicity against the cells (Fig. 1E,F) [26].

### Generation of the Nanofiber Mat With Gradations in Both Fiber Alignment and Mineral Content

Regions I, II, III, and IV were marked on a piece of nanofiber scaffold with a suitable size. A laser intensity of 2 W/cm$^2$ was applied to irradiate the scaffolds for 0, 5, 8, and 10 s, respectively. During irradiation, the unirradiated areas were covered with a mask to prevent welding [17]. The SEM images (Fig. 2A) of the different regions of the nanofiber scaffold revealed the change of nanofibers in a membrane. A structural gradation from an aligned to random arrangement was obtained owing to the different welding extents in each region. Complex gradients of cell types and tissue properties were noted by adjusting the generated strain gradients [11]. The obtained monolithic fiber scaffold was put in the container of increasing mineralization solution to make the hierarchical calcium phosphate coating. The SEM and AFM results in Fig. 2B and Figure S4A illustrate that the surface coating of calcium phosphate gradually increased from region I to region IV. The Young's modulus of the mat surface, from 67.78 ± 2.1 MPa (region I) to 4248.6 ± 339.7 MPa (region IV), had a positive correlation with the number of

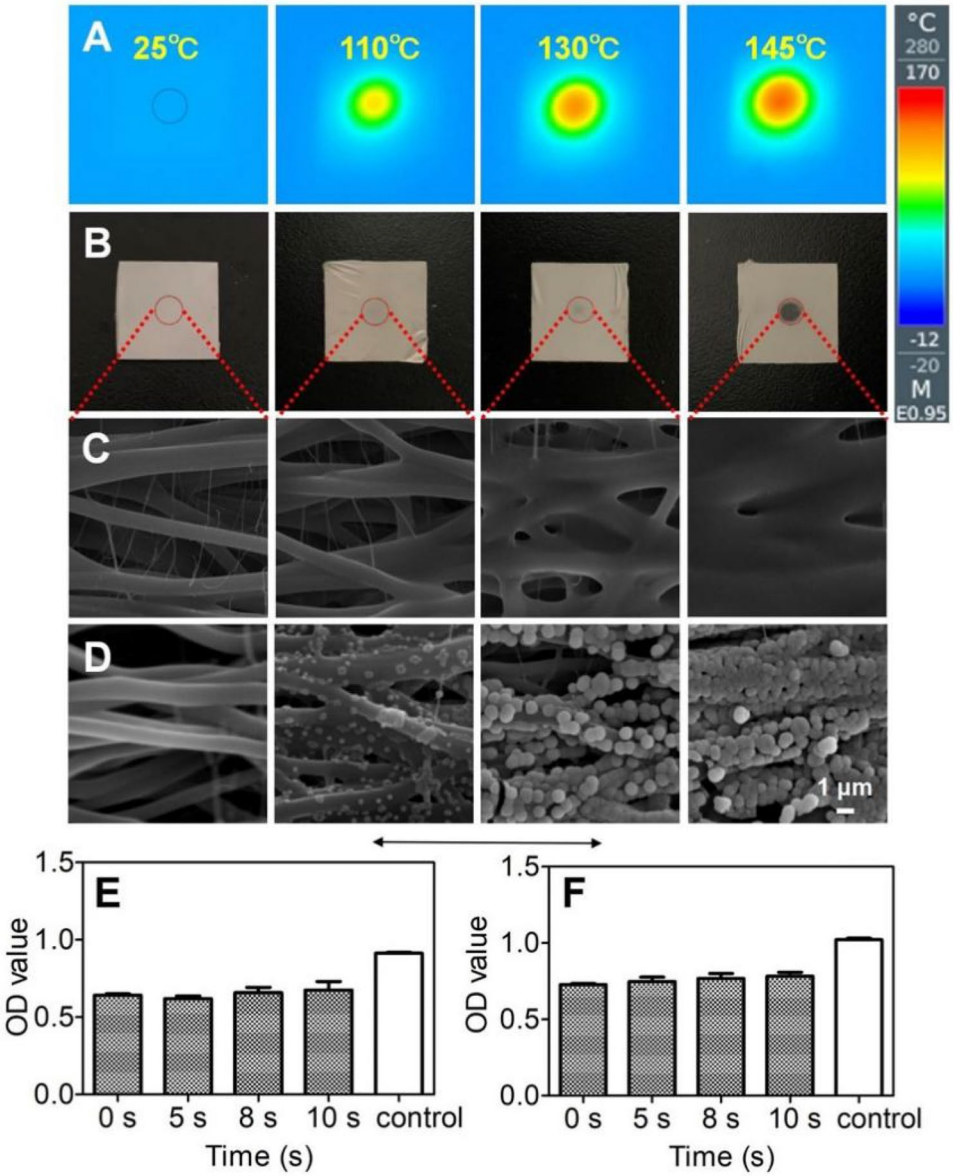


**Fig. 1** Characterizations and cell viability of the PU/ICG nanofiber scaffolds before and post treatment of photothermal welding and mineralization. (**A**) Infrared images, (**B**) photographs, and (**C**) SEM images showing the surface temperatures and morphologies of the nanofiber scaffolds containing 1% ICG after exposure to the laser at an irradiance of 2 W/cm$^2$ for 0, 5, 8, and 10 s (from left to right). (**D**) SEM images showing the corresponding nanofiber scaffolds treated with mineralization solution for 0, 0.5, 1, and 2 h. (**E**) The viability of TDSCs on different nanofiber scaffolds without mineralization after culture for 3 days. (**F**) The viability of tendon derived stem cells on different nanofiber scaffolds post mineralization after culture for 3 days. The arrow represents the direction of fiber orientation

mineral crystals (Fig. 2C). In addition, the result of EDX (Fig. 2D and Figure S5) indicates that the increasing mineralization solution formed continuous gradient mineralization on the surface of the scaffold, which increased the mechanical strengths of the scaffold (Figure S6A).

## TDSC Morphology and Differentiation

F-actin/DAPI staining indicates that the morphology of TDSCs was elongated and arranged regularly in region I, the morphologies changed in regions II and III, and they were disorganized in region IV (Fig. 3A, B). The negative control staining is shown in Figure S6B. Measuring the length and width of the cells revealed that mineralization did not have a significant impact on the changes in cell morphology. For the cells on the scaffold of the PW + GM group, the ratio of the length and breadth of TDSCs in region I was 3.3 times than that in region IV, and the ratio in the case of the PW group was 2.8 times than in region IV (Fig. 3C). The cytoskeleton of the cell could be regulated by the change of the nanofiber alignment on the same nanofiber-based scaffold, which mimicked the cell in the native tendon-bone interface [12]. The proliferation of cells was not significantly changed among PW, PW + GM, and control groups (Fig. 3D). The scaffold was biocompatible without toxicity to cells. Modifications based on the physical microenvironment, particularly the mechanical force and surface morphology, were applied to scaffolds to better mimic the natural tendon microenvironment and induce the differentiation of stem cells toward the tendon cell lineage. Surface morphology is an important

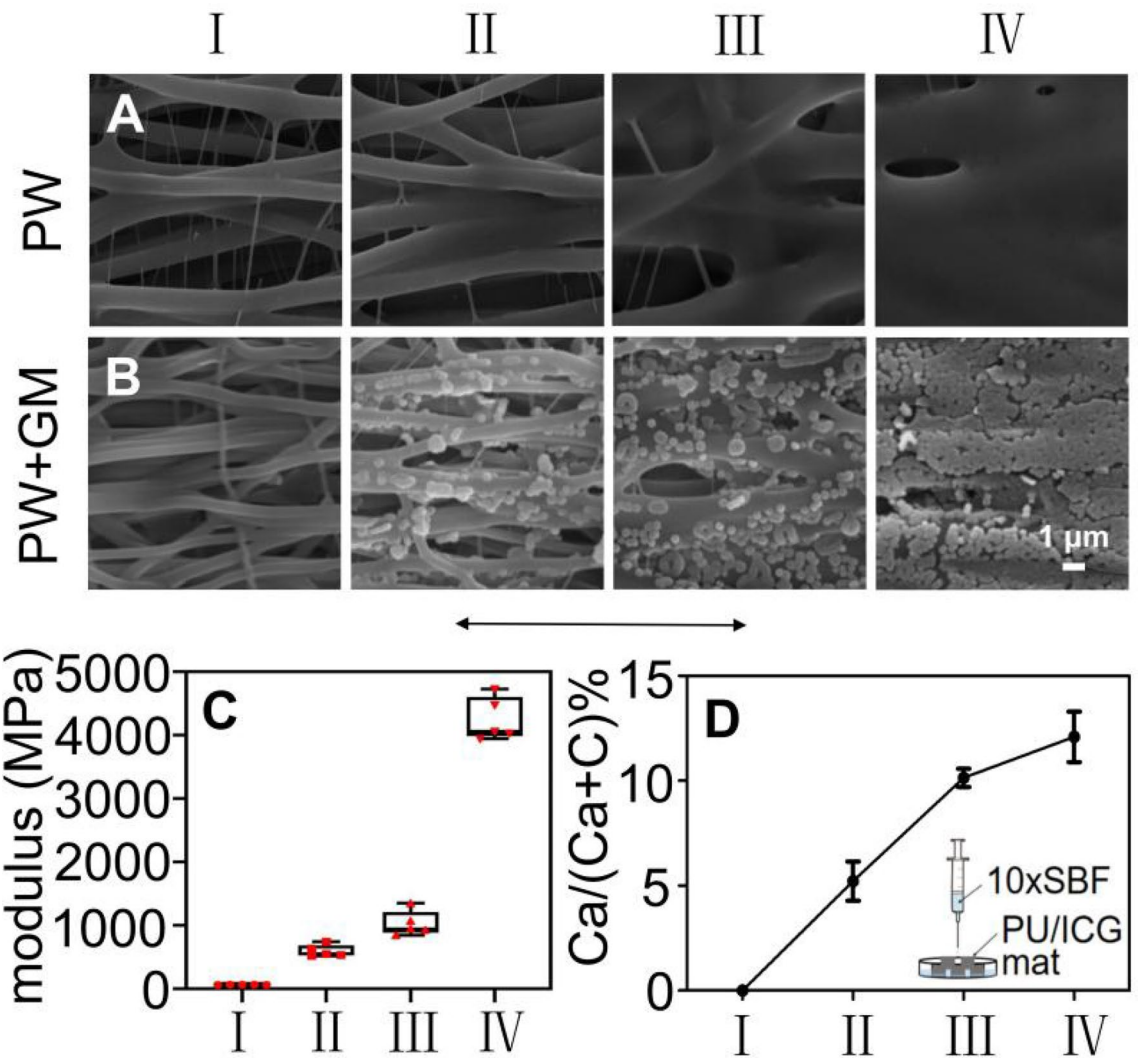


**Fig. 2** Characterizations of the scaffold modified with dual gradients of both surface structure and mineral content. (**A**) SEM images showing the transition from uniaxially aligned to random on the same nanofiber scaffold. (**B**) SEM images of the nanofiber scaffold covered by a graded coating of calcium phosphate at different regions. The mineral content was increased with the transition from aligned to random for the underneath nanofibers. The arrow represents the direction of nanofiber orientation. (**C**) Application of atomic force microscopy to characterize the Young's modulus of different regions on nanofiber scaffolds. Data are expressed as mean ± SD (n = 5). (**D**) Characterization of the mineral content of the different regions on the nanofiber scaffold and schematic illustration showing the generation of a graded coating of calcium phosphate on a nanofiber scaffold. Data are expressed as mean ± SD (n = 4)

factor in the extracellular physical microenvironment. Intracellular signaling and distribution of focal adhesions depend on surface morphology, which can guide cell morphology and motility, regulate cell growth and function, and influence the fate of stem cell differentiation [27–30].

According to the fluorescence intensity (Fig. 4) of TDSCs that were cultured for 14 days, it was inferred that the cells in region I intended to express more Tenascin C protein (green) and less Runx2 protein (red). The cell protein expression in region IV was the opposite. The fluorescence intensity ratios of the two proteins were compared to analyze the difference in their expression in the four regions of the cell (Figure S6C). The negative control staining is depicted in Figure S6D. Runx2 was a landmark factor of osteogenic differentiation, which correlates with the development of calcium pyrroles, and Tenascin C was a landmark factor of tenogenic differentiation, playing a key role in transmitting mechanical forces from one tissue to the next [31–33]. The calcium phosphate coating increased the stiffness of the scaffold and provided signals for TDSCs differentiation toward osteoblasts. It has been proved that the alignment of nanofibers significantly hinders the osteolineage differentiation of human TDSCs cultured under osteogenic conditions [34]. Mechanical signals can be transmitted by a cell through biological factors such as growth factors that bind to receptors on the cell

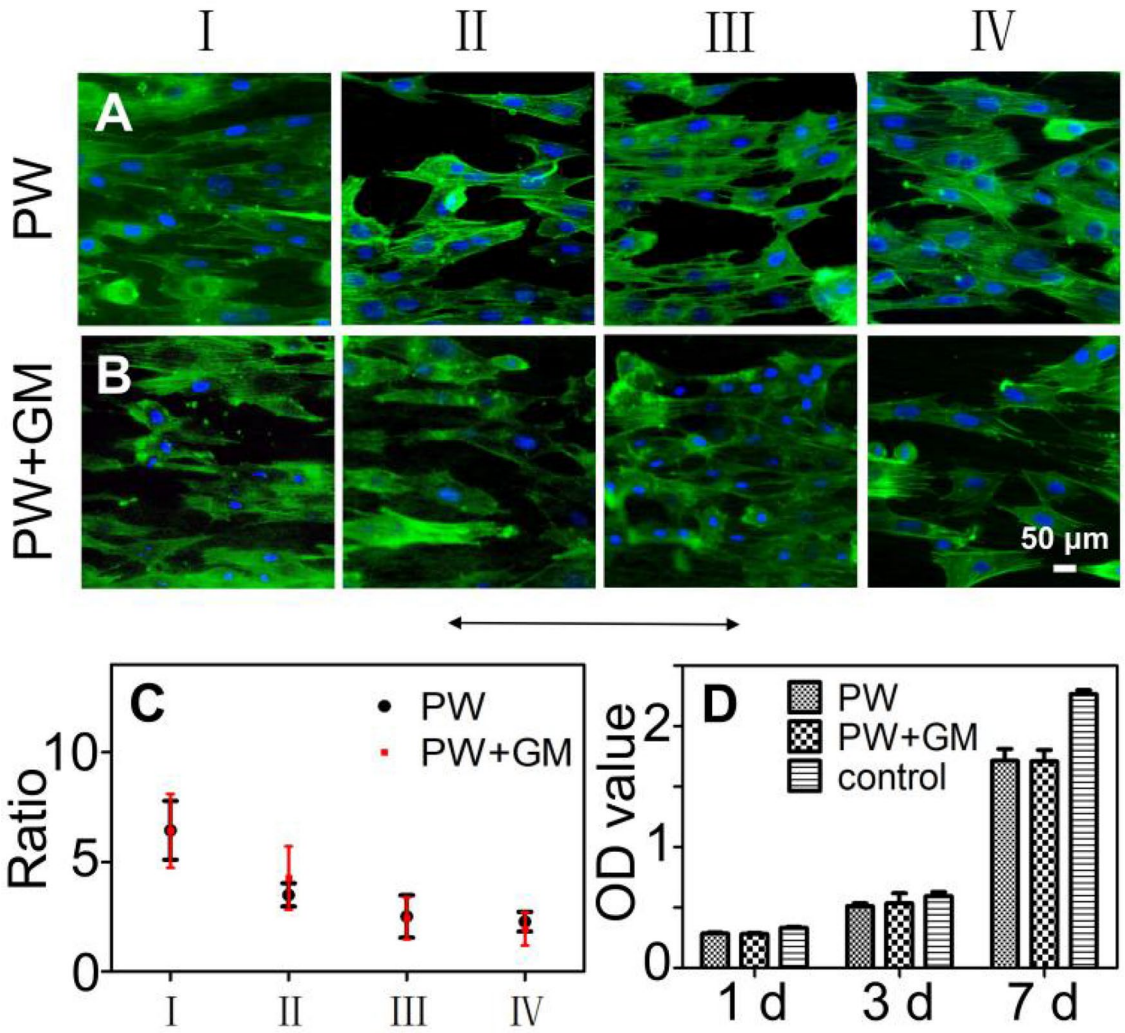


**Fig. 3** The effect of nanofibers and mineralization in different regions on the morphologies and biocompatibility of TDSCs. (**A**, **B**) Fluorescence micrographs showing the morphologies of TDSCs after co-cultured with the nanofiber scaffolds treated by photothermal welding (PW) or photothermal welding plus graded mineralization (PW + GM) for 3 days. The arrow represents the direction of nanofiber orientation. (**C**) The ratio of length and breadth of TDSCs incubated on different regions of the PW and PW + GM groups. (**D**) The proliferation of TDSCs on the different samples tested by CCK-8 assay at 1, 3, and 7 days.

membrane and transmit signals into the cell, thereby initiating several cytoplasmic signaling cascades [35]. The aligned scaffold fibers played a critical role in promoting TDSCs differentiation to tendon cells. It was recapitulated that the organization of ECM could induce the tenogenic differentiation of stem cells, thus leading to cellular organization and matrix deposition resembling native tendon tissues [34]. In conclusion, a nanofiber scaffold with a dual gradient of structure and mineralized coating was successfully prepared. The scaffold had good biocompatibility and adhesion, and it offered an attachment structure to change the morphology in cells and promote regular protein expression, thereby providing a theoretical basis for its role in in vitro experiments.

## In Vivo Repair of Rabbit Rotator Cuff Injury

Scaffolds made of electrospun nanofibers have been considered to be a promising category of carriers for delivering cells [6]. In this regard, such dual-gradient nanofiber scaffolds could also be used to load and deliver exogenous tendon-derived stem cells for in vivo animal studies. Considering future clinical applications, however, there are still some limitations (*e.g.*, costly cell culture steps, long-term isolation and culturing, extensive cell numbers, and cellular immunogenicity) in pre-culturing and implanting exogenous stem cells relative to in situ recruitment of the endogenous stem cells [36, 37]. As such, we used the dual-gradient nanofiber scaffolds for in situ repair of the injured area.

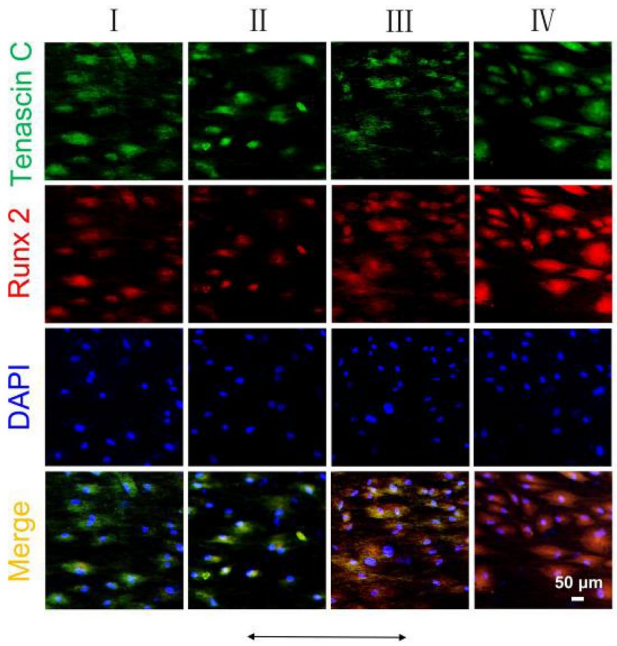


**Fig. 4** Tenogenic and osteogenic differentiation of the TDSCs on the different regions of the dual gradient scaffold. Fluorescence micrographs showing the expression of Tenascin C and Runx2 of TDSCs after co-cultured with the nanofiber scaffold treated by photothermal welding plus graded mineralization for 2 weeks. Cell nucleus were stained by DAPI. Regions I to IV are corresponding to that shown in Fig. 2. The arrow represents the direction of nanofiber orientation

The subscapularis tendon and part of the humerus were obtained at 3 and 6 weeks to observe the healing of the injured tendons (Fig. 5A). None of the animal models got infection. At 3 weeks, the injury in the three groups did not heal significantly, and in 6 weeks, the injuries of subscapularis tendon in PW and PW + GM groups had obvious healing. Especially at 6 weeks, the scaffolds were coated in the hyperplastic tissue at the humerus part. Compared with the control group, the humerus end in the PW and PW + GM groups showed chondroid hyperplasia. H&E and Masson (Figs. 5B and 6A) staining revealed that all of the specimens had poor healing at 3 weeks, when the injuries were clearly visible, and the injuries in three groups were healing well at 6 weeks. The specimens in the PW + GM group produced more connective tissue, and the production of tendon fibers was observed in the middle part (Fig. 6A). The semiquantitative analyses of Masson staining showed that there was more connective tissue appearing in the PW + GM and PW groups (Figure S7A). It was speculated that the fibrous scaffold provided an attachment site for connective tissue proliferation to facilitate tendon repair. The microscopic observation showed that the cell arrangement at the injury site of the PW + GM and PW groups was more orderly than that of the control group. This result suggests that the aligned nanofibers in region I induced tendon-fiber alignment. Sirius red staining (Fig. 6B) illustrated that there was more expression of collagen fibers in the injured sites involving

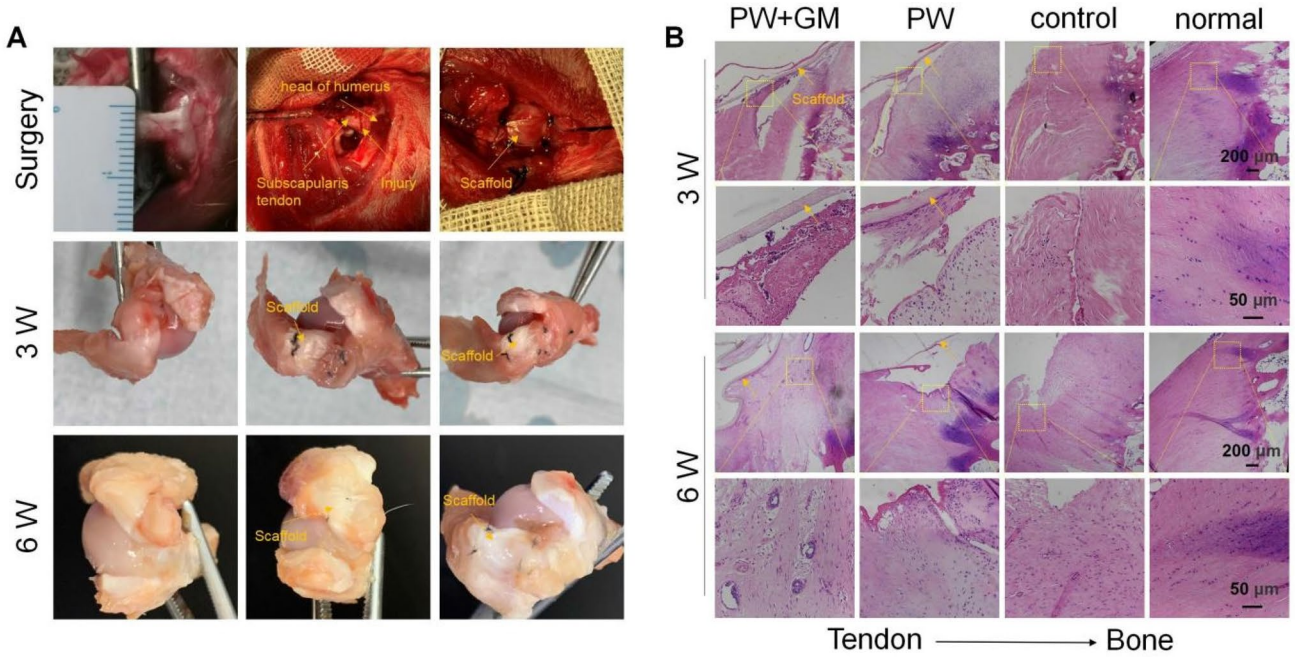


**Fig. 5** In vivo evaluation of H&E staining results at 3- and 6-weeks post implantation. (**A**) Intraoperative and postoperative photographs of the subscapularis tendon: partial injury at the junction of the subscapularis tendon, humerus; implanting the nanofiber scaffold to cover the injury site and samples were explanted after 3 and 6 weeks, respectively. (**B**) H&E staining images of the samples explanted at 3 or 6 weeks. The yellow arrows indicate the nanofiber scaffold

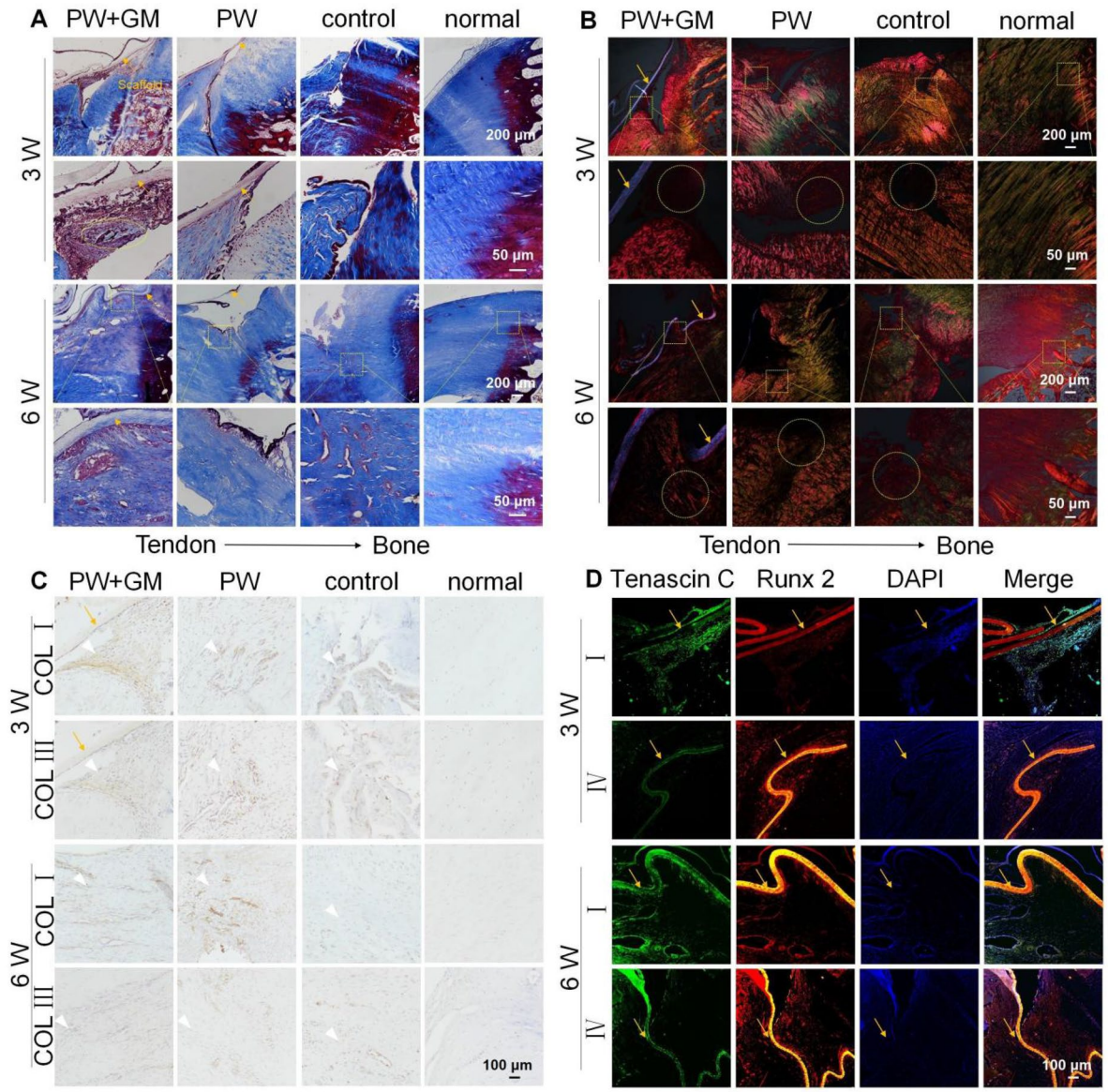


**Fig. 6** Collagen reproduction and the expression of Tenascin C and Runx2 at 3- and 6-weeks post in-vivo implantation. (**A**) Masson staining images of the samples explanted at 3 or 6 weeks. (**B**) Sirius Red staining images of the samples explanted at 3 or 6 weeks. The yellow circles indicate the damage repair parts. (**C**) Immunohistochemical staining of the samples explanted at 3 and 6 weeks. The white arrows point to the damage-repair areas. (**D**) The expression of Tenascin C and Runx2 on regions I and IV after explanted the nanofiber scaffold treated by photothermal welding and graded mineralization at 3 and 6 weeks, respectively. Regions I and IV are corresponding to that shown in Fig. 2. The yellow arrows indicate the nanofiber scaffold

the use of the PW + GM and PW groups at 6 weeks. In the immunohistochemical staining micrographs (Fig. 6C, S7B and C), the expression of type I and III collagen was seen in all of the groups at both time points. The PW + GM and PW groups appeared to express more type I collagen than the control group at 6 weeks (Figure S7B). The expression pattern of collagen I and collagen III is critical in maintaining the tendon structure and function, which is consistent with the natural healing process of the tendon [38]. In the healing of rotator cuff tears, collagen III was mainly produced in the early phase of healing and subsequently replaced by collagen I, which gradually increased [39]. This suggests that the directionally aligned nanofibers contributed to the regular arrangement of cells and promoted the production of type I collagen, which is beneficial for tendon repair. The fluorescence intensities (Fig. 6D) of regions I and IV of the PW + GM group illustrated that the cells around region I expressed more tendon-related protein Tenascin C at 3 and 6 weeks, and the osteogenesis-related protein Runx2 was more expressed around region IV. The negative control

staining is shown in Figure S6E. This result is consistent with the findings we obtained in vitro. There was some limitation on the observation of region II and III. However, region I and IV exhibited a positive effect on the arrangement of cells and fibers and promoted cell differentiation for tendon-bone healing.

The biomechanical test (Fig. 7) proved that there was no significant difference between the PW + GM, PW, and control groups in terms of ultimate failure loads at 3 weeks and ultimate stress at both 3 and 6 weeks. However, the ultimate failure loads in the PW + GM and PW groups at 6 weeks (142 ± 16 N and 135 ± 18 N, respectively) were significantly higher than those in the control group (112 ± 14 N) (*$P < 0.05$) (Fig. 7D). We still tend to make the mineralization gradient such that phosphate calcium provides a tough surface and enhances the overall strength of the membrane. In subsequent studies, the mineralization gradient is also the preferred choice in the progress of developing a three-dimensional scaffold for tendon-bone healing. The mineralized part should be in the bone tunnel to provide chemotaxis for bone ingrowth [40]. Several studies reported the tendon-bone injury repair with a tissue-engineered graft, which was built as a whole composite tissue unit [41, 42]. The graft needs to be obtained from a donor and processed accordingly. The scaffold in this study is convenient to fabricate and easy to preserve. However, it promotes the regeneration of the tendon-bone interface with an assistive effect, which means that it is not able to provide a strong mechanical property to substitute the injured tissue. The scaffolds modified with such dual gradients of both structure and mineralized coating had excellent effects on the morphology and differentiation of TDSCs in vitro and also demonstrated the ability to accelerate the healing of injured rotator cuffs in in vivo experiments.

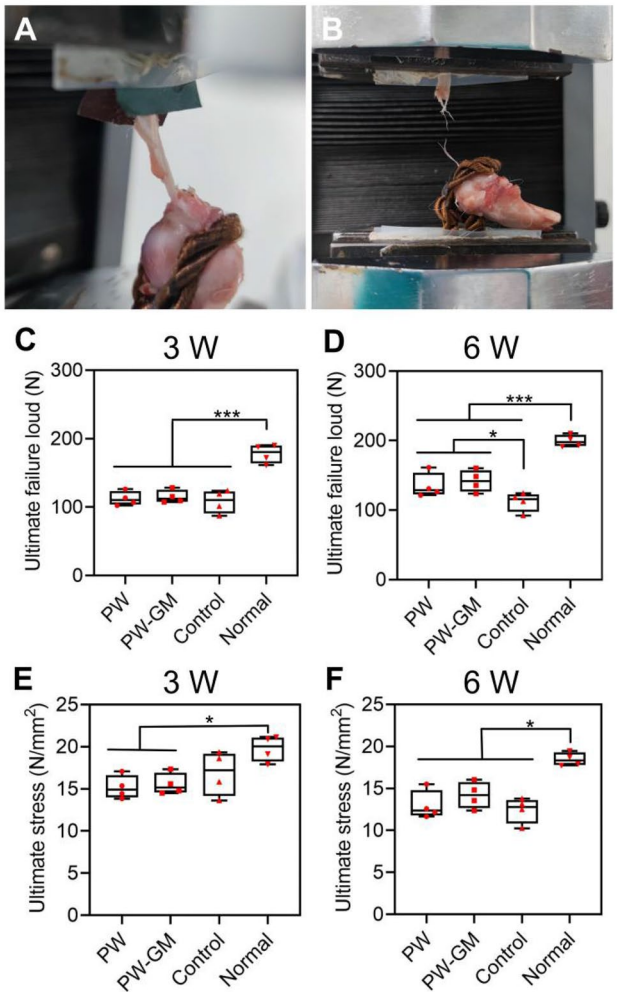


**Fig. 7** Biomechanical tests of the scaffolds at 3- and 6-weeks post in-vivo implantation. (**A**, **B**) Photographs showing the biomechanical test procedure of the samples explanted at 3 or 6 weeks. (**C**, **D**) Ultimate failure load and (**E**, **F**) ultimate stress of the different samples (n = 4). The bar charts represent the mean ± standard deviation; statistically significant at *$P \leq 0.05$, ***$P \leq 0.001$

A number of methods have been developed for generating gradations in structures and/or compositions. In previous studies, specific collections of electrospun nanofibers have been used to obtain an aligned-to-random structure transition [43–45]. As one typical example, a parallel-collector configuration was used to collect electrospun nanofibers [43]. In this case, aligned fibers were bridged between the collectors while randomly oriented fibers were gathered on collector edges. Such transition microstructures showed an influence on cell morphologies, tissue topology, and the formation of enthesis. In a preliminary study, uniaxially aligned nanofibers were treated by graded welding of the fibers along the fiber orientation to form a gradient structure that changed from aligned to random [12]. When seeding BMSCs on such a scaffold, the morphologies of BMSCs were well-controlled from oriented stretching to randomly gathering, corresponding to the fibers underneath. In this example, however, the scaffolds were not used in vivo. In addition to the nanofiber scaffold, a gradient bimetallic (Cu and Zn) ion-based hydrogel made of thiolated gelatin was also designed and successfully used for the reconstruction of tendon-bone insertion using a rat rotator cuff tear model [46]. Considering the biomimetics of both the components and the structures of a native tendon-bone interface, we developed a dual-gradient scaffold that recapitulated both the aligned-to-random transition and the mineral gradation via photothermal welding and dipping/immersion methods. This strategy makes it easy to control the region when changing the fiber structure with the use of a moveable mask, which can be simply extended to use with other polymers if one wants to degrade the scaffold as expected. In terms of the creation of mineral gradation, one can also generate the gradients in other ingredients such as bioactive proteins and growth factors, using this method or the masked electrospray technique, as a coating layer to

manipulate cell behaviors including cell migration and differentiation [47, 48]. We believe the dual-gradient scaffold developed in this study will pave the way for the development of biomaterials for clinical tendon-bone repair and related biomedical applications.

Despite the preliminary outcome in the present study, there were some limitations. For example, the nanofiber scaffold has a two-dimensional structure, hence, it is not suitable for repairing a full-thickness rotator cuff tear. In this regard, attempts are being made to extend this strategy to design a three-dimensional scaffold with spatial gradients in fiber alignment, mineral contents, and cell types. The development of three-dimensional technology offers new ideas for the production of scaffolds [49, 50]. We hope that this technology will be realized in three-dimensional scaffold fabrication and will provide a new way to treat tendon-bone injuries in the future.

## Conclusions

A biomimetic nanofiber scaffold with a dual gradient of structure and mineralized coating was successfully fabricated, and its effect on the morphology change and dissimilar differentiation of TDSCs at different regions of the same scaffold was verified by in vitro experiments in this study. In particular, the prepared scaffold promoted the injured rotator cuff repair in a rabbit model, revealed by the formation of type I collagen and the ultimate tension of the repaired tendon. We believe that this strategy of generating a nanofiber scaffold with dual gradients in both structures and components can also be extended for use with various kinds of three-dimensional scaffolds, providing new candidates for repairing full-thickness ruptures or tendons defects. Following that, we will further develop this type of nanofiber scaffold to produce three-dimensional structures, including more samples for in vivo verification in large animal models.

**Supplementary Information** The online version contains supplementary material available at https://doi.org/10.1007/s42765-022-00154-7.

**Acknowledgements** This research was supported by National Natural Science Foundation of China (31872310, 82001970), Natural Science Foundation of Shandong Province (ZR2019MH097, ZR2021YQ17), Young Elite Scientists Sponsorship Program by CAST (No. YESS20200097), and startup funds from Qingdao University (T.W.).

**Author contributions** CY: methodology, formal analysis, data curation, software, writing-original draft. TW: methodology. HD: formal analysis, writing-original draft. NL: methodology, writing-review & editing. YZ: formal analysis. HJ: methodology, writing-original draft. PZ: methodology. ZS: methodology. ZS: methodology. TW: conceptualization, methodology, resources, supervision, funding acquisition, writing-review & editing. XM: conceptualization, resources. TY: project administration, resources, supervision, funding acquisition.

## Declarations

**Conflict of interest** On behalf of all authors, the corresponding author states that there is no conflict of interest.

## References

1. Tashjian RZ. Epidemiology, natural history, and indications for treatment of rotator cuff tears. *Clin Sports Med* **2012**;*31*:589–604.
2. Iannotti JP, Deutsch A, Green A, Rudicel S, Christensen J, Marraffino S, Rodeo S. Time to failure after rotator cuff repair: a prospective imaging study. *J Bone Joint Surg Am* **2013**;*95*:965–71.
3. Neri BR, Chan KW, Kwon YW. Management of massive and irreparable rotator cuff tears. *J Shoulder Elbow Surg* **2009**;*18*:808–18.
4. Pennisi E. Tending tender tendons. *Science* **2002**;*295*:1011.
5. Butler DL, Juncosa N, Dressler MR. Functional efficacy of tendon repair processes. *Annu Rev Biomed Eng* **2004**;*6*:303–29.
6. Lin Y, Zhang L, Liu NQ, Yao Q, Van Handel B, Xu Y, Wang C, Evseenko D, Wang L. In vitro behavior of tendon stem/progenitor cells on bioactive electrospun nanofiber membranes for tendon-bone tissue engineering applications. *Int J Nanomed* **2019**;*14*:5831–48.
7. Tang Y, Chen C, Liu F, Xie S, Qu J, Li M, Li Z, Li X, Shi Q, Li S, Li X, Hu J, Lu H. Structure and ingredient-based biomimetic scaffolds combining with autologous bone marrow-derived mesenchymal stem cell sheets for bone-tendon healing. *Biomaterials* **2020**;*241*:119837.
8. Chae S, Sun Y, Choi YJ, Ha DH, Jeon IH, Cho DW. 3D cell-printing of tendon-bone interface using tissue-derived extracellular matrix bioinks for chronic rotator cuff repair. *Biofabrication* **2021**;*13*:035005.
9. Rothrauff BB, Yang G, Tuan RS. Tissue-specific bioactivity of soluble tendon-derived and cartilage-derived extracellular matrices on adult mesenchymal stem cells. *Stem Cell Res Ther* **2017**;*8*:133.
10. Xie J, Li X, Lipner J, Manning CN, Schwartz AG, Thomopoulos S, Xia Y. "Aligned-to-random" nanofiber scaffolds for mimicking the structure of the tendon-to-bone insertion site. *Nanoscale* **2010**;*2*:923–6.
11. Kishan AP, Robbins AB, Mohiuddin SF, Jiang M, Moreno MR, Cosgriff-Hernandez EM. Fabrication of macromolecular gradients in aligned fiber scaffolds using a combination of in-line blending and air-gap electrospinning. *Acta Biomater* **2017**;*56*:118–28.
12. Li H, Wu T, Xue J, Ke Q, Xia Y. Transforming nanofiber mats into hierarchical scaffolds with graded changes in porosity and/or nanofiber alignment. *Macromol Rapid Commun* **2020**;*41*:e1900579.
13. Li X, Cheng R, Sun Z, Su W, Pan G, Zhao S, Zhao J, Cui W. Flexible bipolar nanofibrous membranes for improving gradient microstructure in tendon-to-bone healing. *Acta Biomater* **2017**;*61*:204–16.
14. Chen W, Sun Y, Gu X, Cai J, Liu X, Zhang X, Chen J, Hao Y, Chen S. Conditioned medium of human bone marrow-derived stem cells promotes tendon-bone healing of the rotator cuff in a rat model. *Biomaterials* **2021**;*271*:120714.
15. Laranjeira M, Domingues RMA, Costa-Almeida R, Reis RL, Gomes ME. 3D mimicry of native-tissue-fiber architecture guides tendon-derived cells and adipose stem cells into artificial tendon constructs. *Small* **2017**;*13*:1700689.
16. Lui PP, Chan KM. Tendon-derived stem cells (TDSCs): from basic science to potential roles in tendon pathology and tissue engineering applications. *Stem Cell Rev Rep* **2011**;*7*:883–97.

17. Wu T, Li H, Xue J, Mo X, Xia Y. Photothermal welding, melting, and patterned expansion of nonwoven mats of polymer nanofibers for biomedical and printing applications. *Angew Chem Int Ed Engl* **2019**;*58*:16416–21.
18. Li X, Xie J, Lipner J, Yuan X, Thomopoulos S, Xia Y. Nanofiber scaffolds with gradations in mineral content for mimicking the tendon-to-bone insertion site. *Nano Lett* **2009**;*9*:2763–8.
19. Tas AC, Bhaduri SB. Rapid coating of Ti6Al4V at room temperature with a calcium phosphate solution similar to 10× simulated body fluid. *J Mater Res* **2004**;*19*:2742–9.
20. Yamaguchi K, Ditsios K, Middleton WD, Hildebolt CF, Galatz LM, Teefey SA. The demographic and morphological features of rotator cuff disease. A comparison of asymptomatic and symptomatic shoulders. *J Bone Joint Surg Am* **2006**;*88*:1699–704.
21. Isaksson H, Harjula T, Koistinen A, Iivarinen J, Seppänen K, Arokoski JP, Brama PA, Jurvelin JS, Helminen HJ. Collagen and mineral deposition in rabbit cortical bone during maturation and growth: effects on tissue properties. *J Orthop Res* **2010**;*28*:1626–33.
22. Otarodifard K, Wong J, Preston CF, Tibone JE, Lee TQ. Relative fixation strength of rabbit subscapularis repair is comparable to human supraspinatus repair at time. *Clin Orthop Relat Res* **2014**;*472*:2440–7.
23. Grumet RC, Hadley S, Diltz MV, Lee TQ, Gupta R. Development of a new model for rotator cuff pathology: the rabbit subscapularis muscle. *Acta Orthop* **2009**;*80*:97–103.
24. Jing Z, Dexin T, Zihan L, et al. Ultrafast bone-like apatite formation on highly porous poly(l-lactic acid)-hydroxyapatite fibres. *Mater Sci Eng C Mater Biol Appl* **2020**;*116*:111168.
25. Liu W, Lipner J, Xie J, Manning CN, Thomopoulos S, Xia Y. Nanofiber scaffolds with gradients in mineral content for spatial control of osteogenesis. *ACS Appl Mater Interfaces* **2014**;*6*:2842–9.
26. Yang G, Yao Y, Wang X. Comparative study of kerateine and keratose based composite nanofibers for biomedical applications. *Mater Sci Eng C Mater Biol Appl* **2018**;*83*:1–8.
27. Dong Y, Zheng Y, Zhang K, Yao Y, Wang L, Li X, Yu J, Ding B. Electrospun nanofibrous materials for wound healing. *Adv Fiber Mater* **2020**;*2*:212–27.
28. Li Y, Shen Q, Shen J, Ding X, Liu T, He J, Zhu CY, Zhao D, Zhu JD. Multifunctional fibroblasts enhanced via thermal and freeze-drying post-treatments of aligned electrospun nanofiber membranes. *Adv Fiber Mater* **2021**;*3*:1–16.
29. Biehl JK, Yamanaka S, Desai TA, Boheler KR, Russell B. Proliferation of mouse embryonic stem cell progeny and the spontaneous contractile activity of cardiomyocytes are affected by microtopography. *Dev Dyn* **2009**;*238*:1964–73.
30. Brassard JA, Lutolf MP. Engineering stem cell self-organization to build better organoids. *Cell Stem Cell* **2019**;*24*:860–76.
31. Huang AH, Lu HH, Schweitzer R. Molecular regulation of tendon cell fate during development. *J Orthop Res* **2015**;*33*:800–12.
32. Järvinen TA, Kannus P, Järvinen TL, Jozsa L, Kalimo H, Järvinen M. Tenascin-C in the pathobiology and healing process of musculoskeletal tissue injury. *Scand J Med Sci Sports* **2000**;*10*:376–82.
33. Lin B, Srikanth P, Castle AC, Nigwekar S, Malhotra R, Galloway JL, Sykes DB, Rajagopal J. Modulating cell fate as a therapeutic strategy. *Cell Stem Cell* **2018**;*23*:329–41.
34. Yin Z, Chen X, Chen JL, Shen WL, Hieu Nguyen TM, Gao L, Ouyang HW. The regulation of tendon stem cell differentiation by the alignment of nanofibers. *Biomaterials* **2010**;*31*:2163–75.
35. Nourissat G, Berenbaum F, Duprez D. Tendon injury: from biology to tendon repair. *Nat Rev Rheumatol* **2015**;*11*:223–33.
36. He SK, Ning LJ, Yao X, Hu RN, Cui J, Zhang Y, Ding W, Luo JC, Qin TW. Hierarchically demineralized cortical bone combined with stem cell-derived extracellular matrix for regeneration of the tendon-bone interface. *Am J Sports Med* **2021**;*49*:1323–32.
37. Massaro MS, Pálek R, Rosendorf J, Červenková L, Liška V, Moulisová V. Decellularized xenogeneic scaffolds in transplantation and tissue engineering: immunogenicity versus positive cell stimulation. *Mater Sci Eng C Mater Biol Appl* **2021**;*127*:112203.
38. Qu D, Mosher CZ, Boushell MK, Lu HH. Engineering complex orthopaedic tissues via strategic biomimicry. *Ann Biomed Eng* **2015**;*43*:697–717.
39. Hirose K, Kondo S, Choi HR, Mishima S, Iwata H, Ishiguro N. Spontaneous healing process of a supraspinatus tendon tear in rabbits. *Arch Orthop Trauma Surg* **2004**;*124*:374–7.
40. Shi D, Shen J, Zhang Z, Shi C, Chen M, Gu Y, Liu Y. Preparation and properties of dopamine-modified alginate/chitosan-hydroxyapatite scaffolds with gradient structure for bone tissue engineering. *J Biomed Mater Res A* **2019**;*107*:1615–27.
41. Kim BJ, Cho YW, Jo CH. Regeneration of the rotator cuff tendon-to-bone interface using umbilical cord-derived mesenchymal stem cells and gradient extracellular matrix scaffolds from adipose tissue in a rat model. *Acta Biomater* **2020**;*114*:104–16.
42. Baldino L, Cardea S, Maffulli N, Reverchon E. Regeneration techniques for bone-to-tendon and muscle-to-tendon interfaces reconstruction. *Br Med Bull* **2016**;*117*:25–37.
43. Nowlin J, Bismi MA, Delpech B, Dumas P, Zhou Y, Tan GZ. Engineering the hard-soft tissue interface with random-to-aligned nanofiber scaffolds. *Nanobiomedicine* **2018**;*5*:1849543518803538.
44. Xie J, Ma B, Michael PL, Shuler FD. Fabrication of nanofiber scaffolds with gradations in fiber organization and their potential applications. *Macromol Biosci* **2012**;*12*:1336–41.
45. Samavedi S, Vaidya P, Gaddam P, Whittington AR, Goldstein AS. Electrospun meshes possessing region-wise differences in fiber orientation, diameter, chemistry and mechanical properties for engineering bone-ligament-bone tissues. *Biotechnol Bioeng* **2014**;*111*:2549–59.
46. Yang R, Li G, Zhuang C, Yu P, Ye T, Zhang Y, Shang P, Huang J, Cai M, Wang L, Cui W, Deng L. Gradient bimetallic ion-based hydrogels for tissue microstructure reconstruction of tendon-to-bone insertion. *Sci Adv* **2021**;*7*:3816.
47. Wu T, Xue J, Li H, Zhu C, Mo X, Xia Y. General method for generating circular gradients of active proteins on nanofiber scaffolds sought for wound closure and related applications. *ACS Appl Mater Interfaces* **2018**;*10*:8536–45.
48. Xue J, Wu T, Qiu J, Rutledge S, Tanes ML, Xia Y. promoting cell migration and neurite extension along uniaxially aligned nanofibers with biomacromolecular particles in a density gradient. *Adv Funct Mater* **2020**;*30*:2002031.
49. Ma J, Smietana MJ, Kostrominova TY, Wojtys EM, Larkin LM, Arruda EM. Three-dimensional engineered bone-ligament-bone constructs for anterior cruciate ligament replacement. *Tissue Eng Part A* **2012**;*18*:103–16.
50. Elst L, Lima C, Kurtoglu MG, Koraganji VN, Zheng MG, Gumennik A. 3D printing in fiber-device technology. *Adv Fiber Mater* **2021**;*3*:59–75.

**Chenghao Yu** has been a Ph.D. candidate in Clinical Medicine at Qingdao University from 2021 with Prof. Tengbo Yu. He has been working in Prof. Tong Wu's group at Qingdao University from 2020 as a jointly-supervised student. His research interests include the design and fabrication of electrospun nanofiber scaffolds and their use in tendon-to-bone healing.

**Tong Wu** received her Ph.D. in Biomaterials Science from Donghua University in 2018 with Prof. Xiumei Mo. She worked in Prof. Younan Xia's group at the Georgia Institute of Technology from 2016 as a jointly-supervised Ph.D. candidate and then as a postdoctoral fellow until the end of 2019. She is now working as a professor at the medical college of Qingdao University. Her research interests include the development of novel nanomaterials for biomedical, environmental and energy-related applications.

**Xiumei Mo** has held the professor position in Biomaterials at Donghua University since 2004. From 1997 to 2004, she had been a Postdoc fellow in Kyoto University, research fellow in National University of Singapore, and visiting professor in Aachen University. She has been a Committee Member of China Biomaterials Society and Vice Chairman of China Composite Materials Society Super-fine Fiber Branch since 2012. She has got the Science Technical Invention Awards from Shanghai Municipality in 2008, Science and Technology Progress Awards from State Department of People's Republic of China in 2009, and Nature Science Awards from Shanghai Government in 2015.

**Tengbo Yu** obtained his Ph.D. in 2008 from Army Medical University. He is now working as a professor, chief physician, and director of the Knee Protection Department at Qingdao University Affiliated Hospital. He is also the vice president of Qingdao University Affiliated Hospital. His current research interests include tendon-bone healing, cartilage damage and repair, and osteoarthritis treatment.